Evaluation of Doppler-Delay Properties of Diffuse Components in Vehicular Propagation Channels

Yi Zhou[1], Xuefeng Yin[1], Nicolai Czink[2], Thomas Zemen[2], Aihuang Guo[1], and Fuqiang Liu[1]

[1]School of Electronics and Information Engineering, Tongji University, Shanghai, China
[2]Forschungszentrum Telekommunikation Wien (ftw), Vienna, Austria
Email: {2009_zhouyi, yinxuefeng}@tongji.edu.cn, {czink, zemen}@ftw.at, {tjgah, liufuqiang}@tongji.edu.cn

***Abstract*—In this contribution, both numerical and experimental investigations are performed to evaluate the impact of diffuse scattering on the characteristics of vehicular propagation channels in highway environments. The response of a vehicle-to-vehicle (V2V) channel can be composed of discrete specular path components and diffuse scattering components. Simulation results in two V2V scenarios with different settings illustrate the power spectra of the diffuse components induced by the diffuse zone along the highway in delay, Doppler frequency, and in biazimuth (azimuth of arrival and azimuth of departure). Measurement data collected in a highway scenario are processed by using the SAGE (Space-Alternating Generalized Expectation-maximization) algorithm. Results show that the empirical delay-Doppler frequency spectrum of the diffuse components is consistent with the simulated spectrum obtained by using an appropriate setting. This investigation also indicates the necessity of jointly modeling the discrete specular path components and diffuse scattering components for vehicular propagation channels.**

***Index Terms*—Channel modeling, geometry-based, diffuse scattering, and power spectrum.**

I. Introduction

Characteristics of time-variant propagation channels have a great impact on the coverage, capacity, and performance reliability of vehicular communication networks. Accurate and realistic models of propagation channels are crucial for the design and performance optimization of vehicular communication systems. Experimental characteristics of V2V propagation channel were surveyed in [1], and some modeling approaches were summarized as well. In [2], a geometry-based stochastic model was proposed for V2V channels based on the empirical evidence of the contributions of the vehicular channel responses, which consist of the line-of-sight (LOS) components, specular components contributed by discrete scatterers, and the diffuse components contributed by diffuse scatterers.

For the discrete components contributed by individual specular paths, the high resolution algorithms, e.g. SAGE [3] and ESPRIT [4], can be used to estimate the parameters of the paths. Based on the estimation results, stochastic channel models, such as the WINNER models [5] are constructed. However, due to the tremendous amount of unresolvable paths within the component, the generic modeling methods based on specular paths can be very complex to describe the characteristics of diffuse components. We need to find out the physical properties of the diffuse scattering in order to characterize the diffuse components and construct realistic models. In [6], it was observed that the diffuse scattering can contribute more to the capacity of MIMO (Multiple-Input Multiple Ouput) channel than the discrete well-separated paths. Thus, the diffuse component in the channel response should not be neglected. It is necessary to characterize the physical properties for the diffuse components such that the channel response can be described more precisely.

In [7], the power-delay profile of the diffuse component, i.e. the so-called multi-path component, is modeled as an exponential decay function. While the power spectrum of diffuse components in the spatial and delay domain are characterized by series of von-Mises Fisher probability density functions in [8], [9]. The spatial-temporal properties of diffuse components are also addressed in [10]. The results reported in these references provide more insights for characterization of diffuse components. However, these results focus on the expression of the diffuse components in the path-parameter space without analyzing the mechanism for the generation of the diffuse scattering.

Furthermore, the researches conducted in [7], [8], [9], [10] do not cover the characteristics of diffuse components in Doppler frequency-delay domain, which is particularly significant in vehicular channels. Experimental results shown in [2] indicate a specific Doppler frequency-delay profile of the diffuse components from V2V channel measurements. In [11], the power spectra obtained using ray-tracing techniques are compared with those observed in real measurements. It is shown that the ray-tracing techniques at present cannot be used to reproduce correctly the impact of diffuse scattering on the channel responses. Thus, it is essential to propose a reasonable modeling method for characterizing the diffuse scattering in vehicular propagation channels.

This contribution provides an evaluation of the current model of diffuse scattering on highways [2]. Our own simulations based on a geometrical approach are performed to evaluate the Doppler frequency-delay characteristics of diffuse components in vehicular propagation channels in a highway propagation environment. The diffuse scattering is assumed to be caused by many single-bounce scatterers distributed uniformly in two rectangular belts along the highway. The power spectra in delay, Doppler frequency, azimuth of departure and azimuth of arrival are simulated for two V2V propagation scenarios. In the simulations, every single scatterer is assumed to reflect a plane wave with a corresponding attenuation, delay and Doppler shift. Then we process measurement data collected

in a highway environment to validate the simulation results. These studies can provide more insights for understanding the mechanism of the diffuse components and defining suitable approaches for characterizing the diffuse components for vehicular channel modeling.

The organization of this paper is as follows. Section II presents the proposed geometry-based approach for simulating the components of diffuse scattering in the propagation channel. In Section III, two typical V2V propagation scenarios are simulated, and the power spectra of the channel are calculated based on the proposed modeling scheme. In Section IV, the experimental characteristics of vehicular channels in a highway environment are illustrated and compared with simulation results obtained by emulating the real highway vehicular environment. Finally, conclusive remarks are made in Section V.

II. Geometry-based approach for modeling diffuse components

Following the V2V channel model presented in [2], four kinds of components can be found in the response of a V2V propagation channel: the propagation along the line-of-sight (LOS) path between the vehicles in communication, the interactions with stationary discrete (SD) scatterers, the interactions with moving discrete (MD) scatterers, and the effect of diffuse scattering (DI). The spread function of a vehicular channel in delay τ and Doppler frequency ν can be written as

$$h(\nu,\tau) = h_{\mathrm{LOS}}(\nu,\tau) + \sum_{p=1}^{P} h_{\mathrm{SD}}(\nu_{\mathrm{p}},\tau_{\mathrm{p}}) + \sum_{q=1}^{Q} h_{\mathrm{MD}}(\nu_{\mathrm{p}},\tau_{\mathrm{q}}) + \sum_{r=1}^{R} h_{\mathrm{DI}}(\nu_{\mathrm{p}},\tau_{\mathrm{r}}), \quad (1)$$

where P, Q and R denotes the number of components induced by the SD, MD scatterers and the DI effect respectively. For notational conveniences we call these components as the LOS, SD, MD and DI components in the sequel. For high-resolution parameter estimation of the LOS, SD and MD components, the generic specular path model can be used [12], [3], [13]. The local spreads of these components can be estimated by using the clustering methods [14] or the SAGE-based estimator for the power spectrum of the components [8]. Unfortunately, these methods are inappropriate to handle the DI components. In the following, the mechanism for generating the DI components is elaborated by using a geometrical approach which emulates the real propagation in vehicular environments. This would provide more insights for modeling the characteristics of the DI components in vehicular channels.

Fig. 1 depicts the diagram of a vehicular environment. The ribbon in grey represents a multi-lane bidirectional highway. The two rectangular shapes besides the highway denote the diffuse zones which consist of a multitude of scatterers such as plants, bushes, and trees. On the highway, we assume two vehicles which are the transmitter and the receiver respectively,

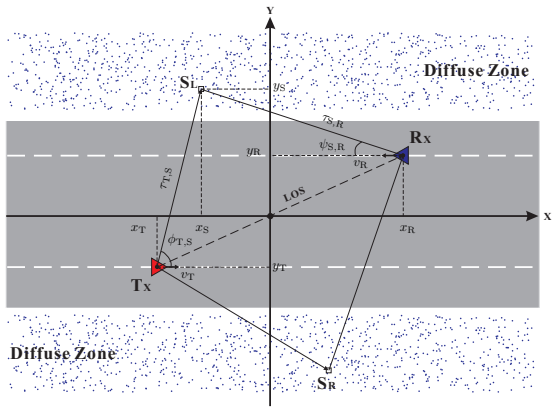

Figure 1. Geometrical model of diffuse components in highway environment.

move at certain speeds in opposite directions towards each other without loss of generality. The LOS component in (1) exists when there is no object blocking the LOS connection. The SD components in (1) are generated by the stationary objects such as buildings, roadsigns and poles along the highway. The MD components are induced by other moving vehicles. We assume that the DI components are generated by the large amount of single-bounce scattering due to the objects in the diffuse zones. It is possible that the surface of the highway can also contribute to the DI components. In this contribution, we use the diffuse zone as an example to analyze the power spectrum of the resulting DI component in delay, Doppler frequency, and biazimuth (Azimuth of Departure and of Arrival) domains. The results can be extended to describe other DI components in the same channel response.

A. Delay and Doppler frequency spread function of a single path in the DI component

As depicted in Fig. 1, for the considered time instance the transmitter and the receiver are located at respectively $(x_{\mathrm{T}}, y_{\mathrm{T}})$ and $(x_{\mathrm{R}}, y_{\mathrm{R}})$. The velocities of the Tx and the Rx are denoted with v_{T} and v_{R} respectively. The rth stationary scatterer S_r is located at $(x_{\mathrm{S}_r}, y_{\mathrm{S}_r})$ within the upper diffuse zone. The azimuth of departure (AoD) and the azimuth of arrival (AoA) of the path induced by this scatterer are represented with $\phi_{\mathrm{T,S}_r}$ and $\psi_{\mathrm{S_r,R}}$ respectively. The delay τ_r of the path can be computed by summing the delay $\tau_{\mathrm{T,S}_r}$ from Tx to the scatterer and the delay $\tau_{\mathrm{S_r,R}}$ from the scatterer to Rx:

$$\tau_r = \tau_{\mathrm{T,S}_r} + \tau_{\mathrm{S_r,R}}. \quad (2)$$

With the assumption that the scatterer is stationary, the Doppler frequency ν_r is calculated as

$$\nu_r = c^{-1}[v_{\mathrm{T}} \cdot \cos\phi_{\mathrm{T,S}_r} + v_{\mathrm{R}} \cdot \cos\psi_{\mathrm{S_r,R}}], \quad (3)$$

with λ denoting the wavelength for the carrier frequency. According to the geometrical constellation shown in Fig. 1, it is straightforward to show that

$$\tau_r = c^{-1}\left[\frac{x_{\mathrm{T}} - x_{\mathrm{S}_r}}{\cos\phi_{\mathrm{T,S}_r}} + \frac{x_{\mathrm{R}} - x_{\mathrm{S}_r}}{\cos\psi_{\mathrm{S_r,R}}}\right], \quad (4)$$

where c is the speed of light. By inserting $\cos\phi_{\mathrm{T,S}_r} = \frac{x_\mathrm{T} - x_{\mathrm{S}r}}{c_0 \cdot \tau_{\mathrm{T,S}_r}}$ and $\cos\psi_{\mathrm{S_r,R}} = \frac{x_\mathrm{R} - x_{\mathrm{S}r}}{c_0 \cdot \tau_{\mathrm{S_r,R}}}$ into Eq. (3) yields

$$\nu_r = \lambda^{-1}\left[\frac{v_\mathrm{T}\cdot(x_\mathrm{T} - x_{\mathrm{S}_r})}{c\cdot\tau_{\mathrm{T,S}_r}} + \frac{v_\mathrm{R}\cdot(x_\mathrm{R} - x_{\mathrm{S}_r})}{c\cdot\tau_{\mathrm{S_r,R}}}\right], \quad (5)$$

Eq. (4) and (5) shows that the location of the path induced by the scatterer in delay and Doppler frequency domain. We need to compute the power associated with the path in order to compute the power spectrum of the DI components in delay and Doppler frequency domain.

B. Power of the path induced by the scatterer

We use a pathloss model to calculate the relative power of the path induced by the scatterer in the diffuse zone. The pathloss considered reads

$$\alpha_r = L_0 + \gamma\cdot 10\log_{10} d_{\mathrm{T,S}_r} + \gamma\cdot 10\log_{10} d_{\mathrm{S_r,R}}, \quad (6)$$

where L_0 denotes the pathloss in dB at the reference distance (usually 1m), γ represents the propagation distance exponent (or attenuation coefficient), $d_{\mathrm{T,S}_r} = c\cdot\tau_{\mathrm{T,S}_r}$ and $d_{\mathrm{S_r,R}} = c\cdot\tau_{\mathrm{S_r,R}}$ denote respectively the distance between Tx and the scatterer and the distance between the scatterer and the Rx. Inserting into (6), we obtain the power calculated for the path with parameters (ν_r, τ_r). Thus, the power spectrum of the DI component can be written as

$$p(\tau,\nu) = p_o\sum_{r=1}^{R} 10^{-\frac{\alpha_r}{10}}\delta(\tau-\tau_r)\delta(\nu-\nu_r) \quad (7)$$

with p_o denoting the transmitted power, and α_r, τ_r and ν_r calculated using (6), (4) and (5) respectively. Notice that α_r, τ_r and ν_r are also the functions of x_{S_r}, $\phi_{\mathrm{T,S}_r}$ and $\psi_{\mathrm{S_r,R}}$. By specifying the distributions of geometric parameters, we can either derive or simulate the power spectrum $p(\tau,\nu)$ for specific DI components.

III. Simulation Studies on the Characteristics of DI Components

In this section, the power spectrum of the DI component induced by the scatterers in the diffuse zone shown in Fig. 1 is simulated for two scenarios referring to different mobility settings for two vehicles. In the first scenario, the two vehicles travel towards each other in different lanes of the highway. In the second scenario, two vehicles travel in same direction in parallel on the same side of the highway. In both scenarios, the speeds of the vehicles are identical and equal 90 km/h.

The environment surrounding the highway is depicted in Fig. 1. The diffuse zone consists of two rectangular belts with width equal to 10 m and length 800 m. In a simulation run, 15000 scatterers are dropped following uniform distribution within each belt. For simplicity, we do not consider the LOS, SD and MD components. Only single-bounce paths induced by the scatterers dropped are simulated. The carrier frequency is 5.2 GHz. The path loss α_r is calculated with $L_0 = 104$ dB and $\gamma = 5.4$. This setting is consistent with the experimental results in [2].

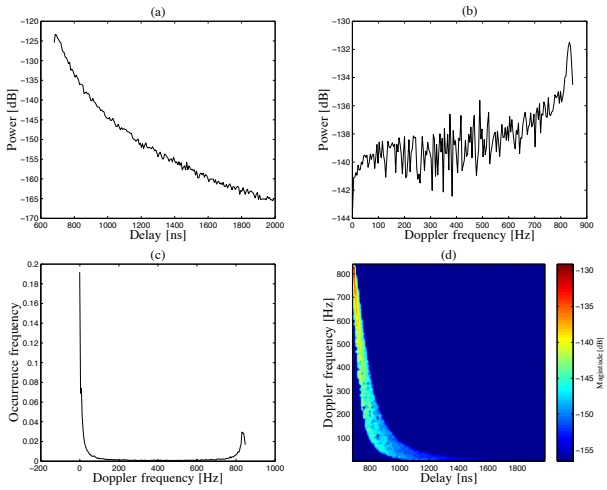

Figure 2. Power spectra of the simulated channel for Scenario i. (a): Power delay spectrum; (b) Power Doppler spectrum; (c) Occurrence frequency of Doppler frequency; (d) Delay-Doppler frequency power spectrum.

A. Scenario i: in opposite direction

As to the first scenario, Fig. 2 (a) and (b) depict the marginal power spectrum of the simulated channel in delay and Doppler frequency, respectively. Fig. 2 (c) illustrates the probability density function of the Doppler frequency per path. Fig. 2 (d) shows the delay-Doppler frequency power spectrum. From Fig. 2 (a), we observe that the power delay spectrum of the simulated DI component exhibits exponential decay, which is similar with the power delay profile of the dense multipath component obtained in [15]. The asymmetric power Doppler frequency spectrum shown in Fig. 2 (b) is similar with the Doppler frequency spectrum derived in [16] for a time-variant scenario where the scatterers are distributed according to a Laplace or Normal distribution around the Tx and the Rx. This is actually true for the simulated scenario where the scatterers uniformly distributed within the diffuse zone result in a bell-shaped distribution around the Tx and the Rx. Fig. 2 (c) also illustrates this phenomenon indirectly.

Fig. 2 (d) depicts the joint delay-Doppler frequency power spectrum of the DI component. Two ribbons with significant spectrum hight are observed in the spectrum, which are induced by the two diffuse zone along the highway. The shapes of the ribbons appear similar. The deviation between them is determined by the width of the highway. In this simulation, the paths with negative Doppler frequencies do not exist. This is because the transmitter and the receiver have the same velocity. It is shown by more simulations that negative Doppler frequency components appear, i.e. these two ribbons will be shifted downwards when the transmitter and the receiver travel in different speeds.

B. Scenario ii: in same direction

Fig. 3 shows the power spectra observed in the simulation for the second scenario, where the transmitter and the receiver travel in parallel at the same speed of $90km/h$. Different from

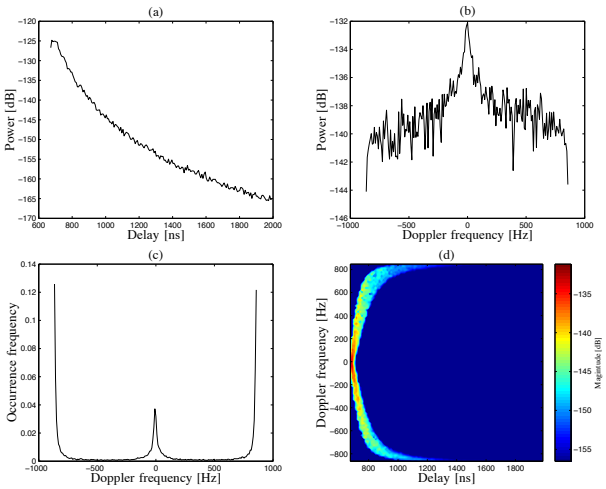

Figure 3. Power spectra of the simulated channel for Scenario ii. (a): Power delay spectrum; (b) Power Doppler spectrum; (c) Occurrence frequency of Doppler frequency; (d) Delay-Doppler frequency power spectrum.

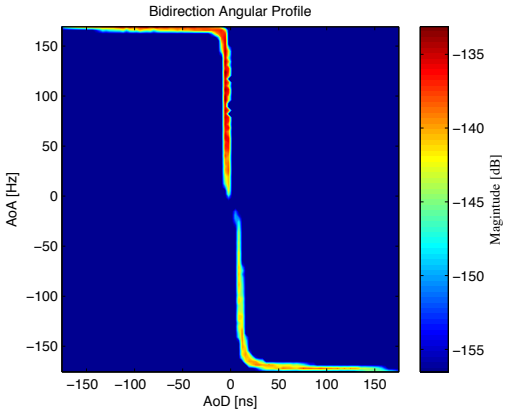

Figure 4. Bi-azimuth power spectrum of the simulated vehicular channel.

the scenario i, the simulated Doppler frequency spectrum is symmetric, which is consistent with the Doppler frequency spectrum derived in [17] for the case where the transmitter and receiver are fixed and all of the scatterers move. Notice that this case is identical with the situation where the transmitter and receiver are moving in parallel at same speed and all scatterers are stationary, as the case simulated in the scenario ii. In the joint delay-Doppler frequency power spectrum shown in Fig. 3 (d), we observe that the power spectrum is very symmetric with respect to the axis with $\nu = 0$. Furthermore, for the case where the speeds of the transmitter and the receiver are different, the power spectrum observed in Fig. 3 (d) are shifted downwards and remain symmetric with respect to the axis with negative Doppler frequency.

Fig. 4 depicts the power spectrum of the DI component in azimuth of departure and azimuth of arrival. It can be observed that the spectrum is symmetric with respect to the point with 0°-AoA and 0°-AoD. This shape is also similar with the simulated bidirection power spectrum of a synthetic micro-cellular environment illustrated in [18]. However, because we only consider one-bounce paths induced by the scatterers confined within two rectangular areas, the obtained bi-azimuth power spectrum in Fig. 4 appears much narrower than that depicted in [18].

IV. Experimental evaluation

In this section, measurement data collected in a V2V environment was processed with the high-resolution estimation method designed based on the SAGE (Space-Alternating Generalized Expectation-maximization) algorithm. The measurement was conducted using the wideband MIMO RUSK-LUND channel sounder on the highway E22 to the east of Lund. During the measurement, the Tx and Rx were located in two cars heading towards each other at the speed of 90 km/h. During the measurement, the Tx and the Rx have clear LOS connection. Fig. 5 illustrates the photograph of the environment taken by a satellite. It can be seen that residence blocks and large buildings are within the vicinity of the highway. Furthermore, trees, bushes and grasses are confined in the diffuse zone along the highway.

Table I lists the configuration parameters of the sounder. Readers are referred to [19] for a detailed description of the sounder. We derived a high-resolution estimator for the parameters of specular paths using the SAGE algorithm. This estimator is applied to extract the delays, Doppler frequencies and complex amplitudes of specular paths from individual segments of the data. Here, a data segment contains $I = 10$ frequency responses of the channel between a specific Tx and a Rx antenna. Each response consists of $N = 792$ subcarriers.

In order to compute the empirical delay-Doppler frequency power spectrum $p(\tau, \nu)$ for the DI component, the LOS, SD and MD components should be removed from the original observed data. From the experimental results shown in [15], we make a realistic assumption that the LOS, SD and MD components are contributed by the waves propagating along the paths with higher amplitude. Heuristically, we choose 60 strongest paths estimated from each data segment to reconstruct the LOS, SD and MD components and subtract from the observation. The power spectrum $\hat{p}(\tau, \nu)$ of the residual signals is calculated based on $S = 20$ segments using the Bartlett beamforming technique [20], i.e.

$$\hat{p}(\tau,\nu) = \frac{1}{SNI}\sum_{s=1}^{S}\sum_{f=f_n}^{f_N}\sum_{t=t_i}^{t_I} |\hat{y}_s(t,f)\exp\{-j2\pi\nu t\} \exp\{-j2\pi f_n\tau\}|^2 \quad (8)$$

Fig. 6 depicts the $\hat{p}(\tau, \nu)$ for the DI component using the data collected when the Tx and Rx were approaching each other. We observed that the significant portion of $\hat{p}(\tau, \nu)$ exhibits a shape similar with that shown in Fig. 2 (d). However, some differences can be observed between these two spectra: *i)* the spectrum $\hat{p}(\tau, \nu)$ is "broken" for $\nu \in [800, 900]$ ns, which is inconsistent with the continuous shape of $p(\tau, \nu)$ simulated; *ii)* the spectrum height of $\hat{p}(\tau, \nu)$ does not decrease as rapidly as shown in $p(\tau, \nu)$. We postulate that the latter difference

Table I
SETTING OF V2V MEASUREMENT CONFIGURATION PARAMETERS.

No.	Specifications	Setting
1	Bandwidth	240 MHz
2	Carrier frequency	5.2 GHz
3	Tx antenna array	4-element uniform circular arrays
4	Rx antenna array	4-element uniform circular arrays
5	Polarization	Dual-polarized
6	Frequency spacing	312.5 KHz
7	Transmit power	27 dBm
8	Snapshot time	102.4μs

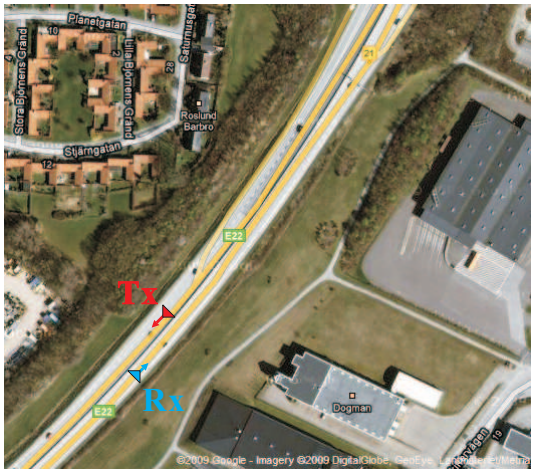

Figure 5. The satellite photo of the measurement highway E22.

is caused by the inappropriate setting of γ when computing the pathloss. The first difference may be due to the facts that the diffuse zone in reality is not as regular and continuous as assumed in the diagram shown in Fig. 1, and additionally, the scatterers within the diffuse zone may not distribute uniformly as supposed in the simulation. Furthermore, single objects with significant physical size existing in the diffuse zone may block the paths of a DI component in such a way that $\hat{p}(\tau, \nu)$ is split into multiple segments. This observation indicates that it is necessary to model the LOS, SD, MD and DI components jointly since the power spectra of these components might be influenced mutually in the vehicular channel.

V. CONCLUSIONS

In this contribution, we proposed a geometrical approach to analyze the diffuse scattering effect in the vehicular channels in the highway propagation environment. On the assumption that the diffuse scattering is caused by a great amount of single-bounce paths induced by scatterers distributed uniformly in two rectangular zones along the highway, we derive the spread function of the channel in Doppler frequency and delay. In the function, each diffuse scatterer can be modeled by a plane wave characterized by delay, Doppler frequency, and the complex-valued attenuation coefficient. Based on this model, we conducted the simulation with two settings for vehicular conditions, and then compared measurement results with that obtained in the simulation. We found that the empirical delay-Doppler frequency power spectrum of the channel is

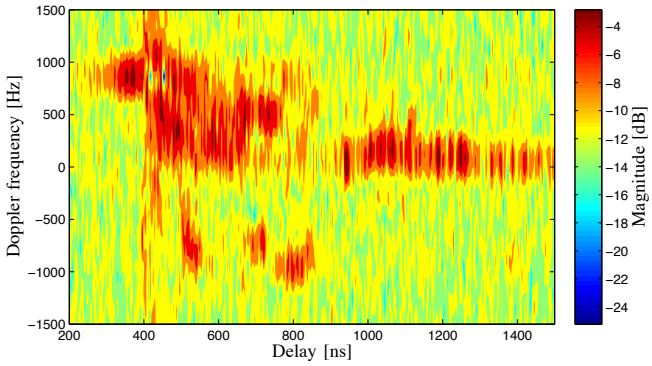

Figure 6. Delay-Doppler frequency Power Spectrum (PS) represented in specular paths estimated from the measurement data.

consistent with the simulated spectrum, which demonstrated that the geometry-based parametric approach is applicable for analyzing the diffuse components.

VI. ACKNOWLEDGEMENT

This work was supported by the National Science & Technology Key Project of China (No.2008ZX03003-005). The work of T. Zemen is supported by the Vienna Science and Technology Fund (WWTF) in the FTW project COCOMINT. The work of N. Czink is supported by the FTW project REALSAFE. FTW is supported by the COMET funding of the Austrian government. The authors would like to acknowledge FTW and Lund University for providing the measurement data.

REFERENCES

[1] A. Molisch, F. Tufvesson, J. Karedal, and C. Mecklenbrauker, "Propagation aspects of vehicle-to-vehicle communications - an overview," in *IEEE Radio and Wireless Symposium, RWS'09*, Jan. 2009, pp. 179–182.

[2] J. Karedal, F. Tufvesson, N. Czink, A. Paier, C. Dumard, T. Zemen, C. F. Mecklenbrauker, and A. F. Molisch, "A geometry-based stochastic mimo model for vehicle-to-vehicle communications," *IEEE Transactions on Wireless Communications*, vol. 8, no. 7, pp. 3646–3657, Jul 2009.

[3] B. H. Fleury, M. Tschudin, R. Heddergott, D. Dahlhaus, and K. I. Pedersen, "Channel parameter estimation in mobile radio environments using the sage algorithm," *IEEE Journal on Selected Areas in Communications*, vol. 17, no. 3, pp. 434–450, Mar. 1999.

[4] R. K. T. Paulraj, A.; Roy, "Estimation of signal parameters via rotational invariance techniques/sup 1/- esprit." Nineteeth Asilomar Conference on Circuits, Systems and Computers, 1985., November 1985, pp. 83–89.

[5] P. Kyösti, J. Meinilä, L. Hentilä, X. Zhao, T. Jämsä, C. Schneider, M. Narandzić, M. Milojević, A. Hong, J. Ylitalo, V.-M. Holappa, M. Alatossava, R. Bultitude, Y. de Jong, and T. Rautiainen, "WINNER II Channel Models D1.1.2 V1.1," no. IST-4-027756 WINNER II, D1.1.2 V1.1, 11 2007.

[6] D. Asztély and B. Ottersten, "The effects of local scattering on direction of arrival estimation with MUSIC," *IEEE Transactions on Signal Processing*, vol. 47, no. 12, pp. 3220–3234, Dec. 1999.

[7] A. Richter, J. Salmi, and V. Koivunen, "Distributed scattering in radio channels and its contribution to mimo channel capacity," in *The First European Conference on Antennas and Propagation, EuCAP 2006*, Nov. 2006, pp. 1–7.

[8] X. Yin, T. Pedersen, N. Czink, and B. H. Fleury, "Parametric characterization and estimation of bi-azimuth and delay dispersion of individual path components," in *The First European Conference on Antennas and Propagation, EuCAP 2006*, Oct. 2006.

[9] X. Yin, L. Liu, D. Nielsen, T. Pedersen, and B. Fleury, "A sage algorithm for estimation of the direction power spectrum of individual path components," Nov. 2007, pp. 3024–3028.

[10] J. Salmi, A. Richter, and V. Koivunen, "Detection and tracking of mimo propagation path parameters using state-space approach," *IEEE Transactions on Signal Processing*, vol. 57, no. 4, pp. 1538–1550, Apr. 2009.

[11] J. Medbo, H. Hallenberg, and J.-E. Berg, "Propagation characteristics at 5 ghz in typical radio-lan scenarios," in *IEEE 49th Vehicular Technology Conference*, Jul 1999, pp. 185–189.

[12] M. Steinbauer, A. Molisch, and E. Bonek, "The double-directional radio channel," *IEEE Antennas and Propagation Magazine*, vol. 43(4), pp. 51–63, 2001.

[13] X. Yin, B. Fleury., P. Jourdan, and A. Stucki., "Polarization estimation of individual propagation paths using the sage algorithm," *14th IEEE Proceedings on Personal, Indoor and Mobile Radio Communications, PIMRC 2003*., vol. 2, pp. 1795–1799, Sept. 2003.

[14] N. Czink, X. Yin, H. Özcelik, M. Herdin, E. Bonek, and B. Fleury, "Cluster Characteristics in a MIMO Indoor Propagation Environment," *IEEE Transactions on Wireless Communications*, vol. 6, no. 4, pp. 1465–1475, 2007.

[15] A. Richter, "Estimation of radio channel parameters: Models and algorithms," *Ph.D. Dissertation, Technische Universität Ilmenau, Verlag ISLE*, 2005.

[16] H. Rad, S. Gazor, and P. Shariatpanahi, "Non-fixed scatterers and their effects on mimo multicarrier fading communication channels," in *IEEE Global Telecommunications Conference, GLOBECOM '07*, Nov. 2007, pp. 3765–3769.

[17] S. Thoen, L. Van der Perre, and M. Engels, "Modeling the channel time-variance for fixed wireless communications," *IEEE Communications Letters*, vol. 6, no. 8, pp. 331–333, Aug 2002.

[18] B. H. Fleury, X. Yin, and A. Kocian, "Impact of the propagation conditions on the properties of MIMO channels," in *Proceedings of International Conference on Electromagnetics in Advanced Applications (ICEAA)*, September 2003, pp. 783–786.

[19] A. Paier, J. Karedal, N. Czink, C. Dumard, T. Zemen, F. Tufvesson, A. F. Molisch, and C. F. Mecklenbräuker, "Characterization of vehicle-to-vehicle radio channels from measurements at 5.2 ghz," *Wireless Personal Communications, Springer Science*, vol. 50, no. 1, pp. 19–32, Jul 2009.

[20] M. Bartlett, "Smoothing periodograms from time series with continuous spectra," *Nature*, vol. 161, 1948.